

## Interactions and disorder in 2D graphite sheets

Francisco Guinea<sup>a</sup>, M. Pilar López-Sancho<sup>a</sup>, and María A. H. Vozmediano<sup>b</sup>

<sup>a</sup>Instituto de Ciencia de Materiales de Madrid, CSIC, Cantoblanco, E-28049 Madrid, Spain.

<sup>b</sup>Departamento de Matemáticas, Unidad Asociada CSIC-UC3M, Universidad Carlos III de Madrid, E-28911 Leganés, Madrid, Spain

### 1. Introduction

Graphite has attracted a lot of recent attention due to the growing evidence that, in many cases, it shows anomalous magnetic and transport properties<sup>1</sup>. The understanding of these features is a significant challenge. Theoretical models for the electronic structure[1] were developed under the assumption that graphite could be described using the Landau theory of a Fermi liquid, although it is assumed that the number of carriers is low.

The theoretical possibility of ferromagnetism in disordered graphite samples was raised long ago[2]. The underlying mechanism is the existence of unpaired spins at defects, induced by a change in the coordination of the carbon atoms (see below). Experimental evidence showing that the lifetimes of the quasiparticles in graphite were not consistent with Fermi liquid theory were reported in[3]. A theoretical model explaining these experiments was suggested in[4]. The model used was based on the existence of incompletely screened electron–electron interactions. In follow up work[5], the analysis was extended in order to include the role of disorder(see also[6]), which is known experimentally to play an important role in relation to the existence of anomalous magnetic properties.

The present work discusses theoretical models which address the effects of electron–electron interactions and disorder in graphene planes following the analysis in[5,6]. The starting point for the study is a simple tight-binding model for the electronic structure, outlined in the next section. Then, a discussion of the interesting features induced by the unscreened Coulomb interaction is presented. The unusual features of the model are emphasized. It is shown that the standard perturbative treatments used in condensed matter theory fail, and a more refined Renormalization Group approach is required. Then, a theoretical framework which allows us to extend the model to many types of disorder, following the approach in[7] for the fivefold rings of the fullerenes, is discussed. The following section analyzes the combined effects of disorder and interactions. A brief discussion of models which may explain the large anisotropy observed in very pure samples of graphite[8], using the theoretical framework explained in[9] is presented next. This work ends with a section highlighting the most interesting conclusions.

---

<sup>1</sup>See other contributions in this volume.

We do not pretend to cover the large and rapidly growing experimental literature on the magnetic properties of graphite and related compounds. This work is extensively covered in other chapters of this volume.

It is worth mentioning that the electronic structure of graphite leads to theoretical models of significant interest for the ongoing quest of understanding strongly correlated systems. This work tries to underline also this aspect of the current work on graphite and related compounds. Because of this reason, we also include a brief summary of the technical aspects of the calculations. We hope that this will not be discourage readers willing just to grasp the main ideas of the work reported here.

## 2. The electronic structure of graphene sheets.

### 2.1. Description of the conduction band.

Graphite, a three dimensional (3D) carbon-based material, presents a layered and highly anisotropic structure, the interaction between two adjacent layers being considerably smaller than the intralayer interactions due to the large layer-layer separation,  $3.35\text{\AA}$  when compared to the nearest-neighbor distance between the carbon atoms  $a = 1.42\text{\AA}$ . In the planes, graphite exhibits semimetallic behavior, and it presents a very weak electrical conductivity along the perpendicular axis.

In the following, we consider the electronic structure of a single graphite sheet, graphene. In the 2D graphite the in-plane  $\sigma$  bonds are formed from  $2s$ ,  $2p_x$  and  $2p_y$  orbitals hybridized in a  $sp^2$  configuration, while the  $2p_z$  orbital, perpendicular to the layer, builds up covalent bonds, similar to the ones in the benzene molecule. The  $\sigma$  bonds give rigidity to the structure, while the  $\pi$  bonds give rise to the valence and conduction bands. The electronic properties around the Fermi energy of a graphene sheet can be described by a tight binding model with only one orbital per atom, the so-called  $\pi$ -electron approximation, because, as stated above, the  $\pi$  covalent bonds are determinant for the electronic properties of graphite and there are no significant mixing between states belonging to  $\sigma$  and  $\pi$  bands in 2D graphite. Within this approximation a basis set is provided by the Bloch functions made up of the  $2p_z$  orbitals from the two inequivalent carbon atoms A and B which form the unit cell of the graphite hexagonal lattice. Considering only nearest-neighbor interactions each atom A of a sublattice has three nearest-neighbors B which belong to the other sublattice [10].

### 2.2. Tight-binding model.

The nearest-neighbor tight binding approach reduces the problem to the diagonalization of the one-electron Hamiltonian

$$\mathcal{H} = -t \sum_{\langle i,j \rangle} a_i^+ a_j \quad (1)$$

where the sum is over pairs of nearest neighbors atoms  $i, j$  on the lattice and  $a_i, a_j^+$  are canonically anticommuting operators

$$\{a_i, a_j\} = \{a_i^+, a_j^+\} = 0, \{a_i, a_j^+\} = \delta_{ij} \quad (2)$$

The eigenfunctions and eigenvalues of the Hamiltonian are obtained from the equation

$$\begin{pmatrix} \epsilon & -t \sum_j e^{iak_{\mathbf{u}_j}} \\ -t \sum_j e^{iak_{\mathbf{v}_j}} & \epsilon \end{pmatrix} \begin{pmatrix} C_A \\ C_B \end{pmatrix} = E(\mathbf{k}) \begin{pmatrix} C_A \\ C_B \end{pmatrix}, \quad (3)$$

where  $\mathbf{u}_j$  is a triad of vectors connecting an A atom with its B nearest neighbors and  $\mathbf{v}_j$  the triad of their respective opposites,  $a$  is the distance between carbon atoms and  $\epsilon$  is the  $2p_z$  energy level, taken as the origin of the energy. The eigenfunctions, expanded as a linear combination of the atomic orbitals from the two atoms forming the primitive cell, are determined by the coefficients  $C_A$  and  $C_B$  solutions of equation (3). The eigenvalues of the equation give the energy levels whose dispersion relation is

$$E(\mathbf{k}) = \pm t \sqrt{1 + 4 \cos^2 \frac{\sqrt{3}}{2} ak_x + 4 \cos \frac{\sqrt{3}}{2} ak_x \cos \frac{3}{2} ak_y}, \quad (4)$$

in which the two signs define two energy bands: the lower half called the bonding  $\pi$  band and the upper half called the antibonding  $\pi^*$  bands, which are degenerate at the  $\mathbf{K}$  points of the Brillouin zone. Within the  $\pi$  electron approximation each site of the graphite honeycomb lattice yields one electron to the Fermi sea and the band is at half-filling. Since each level of the band may accommodate two states due to the spin degeneracy, and the Fermi level turns out to be at the midpoint of the band, instead a whole Fermi line, the 2D honeycomb lattice has six isolated Fermi points which are the six vertices of the hexagonal Brillouin zone, two of which are inequivalent. The lower branch of the dispersion relation is shown in Figure 1. The calculation of the density of states shows that, at the Fermi level, the density of states is zero therefore, the 2D graphite is a semiconductor of zero gap. The existence of a finite number of Fermi points at half-filling has important consequences in the description of the spectrum around the Fermi level. The low energy excitations can be studied by taking the continuum limit at any two independent Fermi points. As long as the number of the Fermi points is finite, the outcome is that a simple field theory suffices to describe the electronic spectrum of large honeycomb lattices. The continuum limit can be taken by scaling of dimensionful quantities since we are dealing with a free theory. Taken into account the parameter  $a$ , the distance between carbon atoms, and expanding the 2x2 operator (3) at any of two independent Fermi points, we have

$$\mathcal{H} = \begin{pmatrix} 0 & -t \sum_j e^{iak_{\mathbf{u}_j}} \\ -t \sum_j e^{iak_{\mathbf{v}_j}} & 0 \end{pmatrix} \approx -\frac{3}{2}ta \begin{pmatrix} 0 & \delta \mathbf{k}_x + \delta \mathbf{k}_y \\ \delta \mathbf{k}_x - \delta \mathbf{k}_y & 0 \end{pmatrix} + O((a\delta \mathbf{k})^2). \quad (5)$$

The scaling

$$\lim_{a \rightarrow 0} \mathcal{H} = -\frac{3}{2}t\sigma^T \delta \dot{\mathbf{k}} \quad (6)$$

determines the effective Hamiltonian in the continuum limit, which turns out to be the Dirac operator in two dimensions. The same result is obtained at any of the six  $\mathbf{K}$  points of the Brillouin zone, therefore, given the existence of the two independent Fermi points,

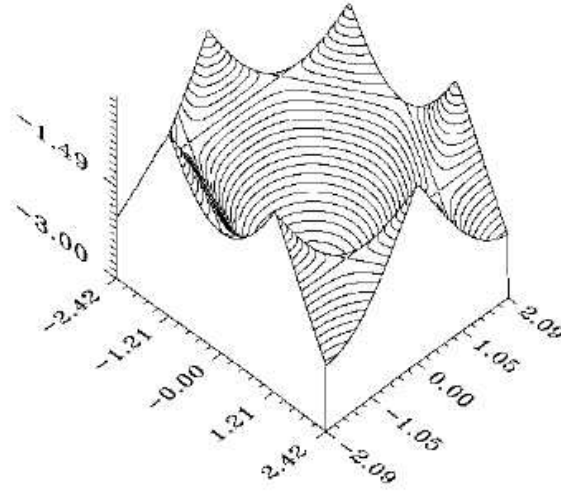


Figure 1. Lower branch of the electronic dispersion relation. The cusps appear at the six corners of the first Brillouin zone.

we conclude that the low energy excitations of the honeycomb lattice at half filling are described by an effective theory of the two-dimensional Dirac spinors. This result is at odds with the more standard continuum approximation to lattice theories in condensed matter physics, the effective mass theory. In this theory, a quadratic dispersion relation at high symmetry points of the Brillouin zone gives rise to an effective Schrödinger equation, with one parameter, the mass, chosen to reproduce the exact curvature. Only one dimensional systems and three dimensional semiconductors with the diamond structure and no gap, are known to give rise to the Dirac equation.

### 3. The long range Coulomb interactions in graphite.

#### 3.1. Screening in graphite.

The band structure of a graphene plane, as discussed in the preceding section, leads to semimetallic behavior, as the density of states vanishes at the Fermi energy. In a semimetal the long range Coulomb interactions are not screened. The system, however, has no gap, and we can expect that the electron–electron interactions modify significantly the electronic structure near the Fermi energy.

The role of the interactions can be appreciated if their effect is analyzed within perturbation theory. One obtains corrections to the Fermi velocity and to the density of states which show a logarithmic dependence on the temperature or other energy scale at which these quantities are measured. This dependence implies that perturbation theory cannot be used at sufficiently low energies. On the other hand, it allows us to use the Renormalization Group approach. In physical terms, the procedure amounts to defining effective couplings which have a non trivial energy or temperature dependence. The dependence of these couplings on energy can be calculated using well tested techniques developed in the study of Quantum Field Theory, as explained below.

### 3.2. Renormalization group analysis of the interactions.

The implementation of the renormalization group (RG) scheme in condensed matter systems[11] has been a theoretical hallmark for correlated electron systems in the last decade. The condensed matter approach shares ideas from both the critical phenomena and the quantum field theory approaches. The main issue is that for special systems (critical, renormalizable) the low-energy physics is governed by an effective Hamiltonian made of a few marginal interactions that can be obtained from the microscopic high-energy Hamiltonian in a well prescribed manner.

Interactions are classified as relevant, irrelevant or marginal according to their scale dimensions. These dimensions determine whether they grow, decrease, or acquire at most logarithmic corrections at low energies. The effective coupling constants of a model at intermediate energies by "integrating out" high-energy modes even if there is no stable fixed point at the end of the RG flow. The Luttinger and Fermi liquids are identified as infrared fixed points of the RG applied to an interacting metallic system in one or more dimensions respectively.

The main difficulty of the RG approach in condensed matter systems in dimensions greater than one lies on the extended nature of the "vacuum" i.e., of the Fermi surface what makes the issue of scaling rather tricky. The situation is aggravated by the fact that the Fermi surface itself is changed by the interactions, i.e. changes along the RG flow.

The Hamiltonian (8) is the perfect model for Renormalization Group (RG) calculations. It is scale invariant and does not have the complications of an extended Fermi surface. The model is similar to the  $D = 1$  electron system[13] in that it has Fermi points and linear dispersion around them. Its two-dimensional nature manifests itself in the fact that in this case four fermion interactions are irrelevant instead of marginal. The only interaction that may survive at low energies is the long (infinite) range Coulomb interaction, unscreened because of the vanishing density of states at the Fermi point.

The RG analysis of the model is as follows:

The scaling dimension of the interactions are determined by these of the fermion fields which can be read off from the non interacting hamiltonian,

$$\mathcal{H}_0 = \hbar v_F \int d^2\mathbf{r} \bar{\Psi}(\mathbf{r})(i\sigma_x\partial_x + i\sigma_y\partial_y)\Psi(\mathbf{r}) \quad (7)$$

Because of the linear dispersion of the electronic states, we can use  $v_F$  to transform time scales into length scales. Then, we can express the dimensions of all physical quantities in terms of lengths. Within this convention, the Hamiltonian has dimensions of energy ( $l^{-1}$ ). This fixes the scale dimension of the electronic fields to  $[\Psi] = l^{-1}$ , where  $l$  defines a length. This also ensures that the free Hamiltonian is scale invariant. We can then readily determine the relevance of the interactions to lowest order (tree level). The interacting Hamiltonian including the two Fermi points ( $i, i'$ ) and the spin degrees of freedom ( $s, s'$ ) is

$$\begin{aligned} \mathcal{H}_{int} = & \sum_{i,i';s,s'} \frac{e^2}{2\pi} \int d^2r_1 \int d^2r_2 \frac{\bar{\Psi}_{i,s}(\vec{r}_1)\Psi_{i,s}(\vec{r}_1)\bar{\Psi}_{i',s'}(\vec{r}_2)\Psi_{i',s'}(\vec{r}_2)}{|\vec{r}_1 - \vec{r}_2|} + \\ & + \sum_{s,s';i,i'} u_{i,s;i',s'} \int d^2r \bar{\Psi}_{i,s}(\vec{r})\Psi_{i,s}(\vec{r})\bar{\Psi}_{i',s'}(\vec{r})\Psi_{i',s'}(\vec{r}) . \end{aligned} \quad (8)$$

A naive power counting analysis shows that the Coulomb potential (first term in eq. (8)) defines a dimensionless, marginal coupling, while the four Fermi couplings  $u$ 's scale as  $l^{-1}$ , and are irrelevant at low energies. This effect can be traced back to the vanishing density of states at the Fermi level.

The next step of the RG consists in analyzing the renormalization of the parameters describing the system when quantum corrections are included. When renormalized, the marginal interactions can either grow, driving the system away of its free fixed point – this is the case of an attractive four Fermi interaction in the Fermi liquid case –, decrease and become irrelevant (repulsive interactions in the Fermi liquid), or stay marginal in which case they define the theory (forward scattering in a Fermi liquid and the related Landau parameters). Our model differs from the usual Fermi liquid analysis of [11] on the fact that our interaction is a long ranged (infinite range) unscreened Coulomb interaction, a case that lies away of the Fermi liquid hypothesis.

Following the quantum field theory nature of the model, we replace the instantaneous Coulomb interaction of eq. (8)

$$\mathcal{H}_C = \frac{e^2}{4\pi v_F} \int d^2\mathbf{r}_1 \int d^2\mathbf{r}_2 \frac{\bar{\Psi}(\mathbf{r}_1)\Psi(\mathbf{r}_1)\bar{\Psi}(\mathbf{r}_2)\Psi(\mathbf{r}_2)}{|\mathbf{r}_1 - \mathbf{r}_2|} \quad (9)$$

where  $g = e^2/4\pi v_F$  is the dimensionless coupling constant, by a local gauge interaction through a minimal coupling.

$$L_{int} = g \int d^2x dt j^\mu(x, t) A_\mu(x, t) ,$$

where the electron current is defined as

$$j^\mu = (\bar{\Psi}\gamma^0\Psi, v_F\bar{\Psi}\boldsymbol{\gamma}\Psi) ,$$

the three  $\gamma$  matrices ( $\gamma^{0,1,2}$ ) are appropriate combinations of the Pauli matrices. The full Hamiltonian is then that of (non-relativistic) quantum electrodynamics in two spacial dimensions, a model used also in the physics of nodal states of d-wave superconductors:

$$\mathcal{H} = \hbar v_F \int d^2\mathbf{r} \bar{\Psi}(\mathbf{r}) \gamma^\mu (\partial_\mu - igA_\mu) \Psi(\mathbf{r}) . \quad (10)$$

The RG analysis proceeds with the computation of the renormalization of the parameters of the model. The Feynman diagrams building blocks are the free electron and photon propagators:

$$G_0(\omega, \mathbf{k}) = i \frac{-\gamma^0\omega + v_F\boldsymbol{\gamma} \cdot \mathbf{k}}{-\omega^2 + v_F^2\mathbf{k}^2 - i\epsilon} , \quad \Pi_{\mu\nu}^0(r_1, r_2) = -i\delta_{\mu\nu} \int \frac{d^4k}{(2\pi)^4} \frac{e^{-i\omega(t_1-t_2)} e^{i\mathbf{k}(\mathbf{x}_1-\mathbf{x}_2)}}{-\omega^2 + \mathbf{k}^2 - i\epsilon} .$$

The electron self-energy  $\Sigma(\omega, \mathbf{k})$  defined by the equation  $G^{-1} = G_0^{-1} - \Sigma$ , is renormalized by the Feynman diagrams of Fig. 2. It contains the following physical information:

- The density of states  $n(\omega) = Im \int d^2\mathbf{k} \text{tr}G(\omega, \mathbf{k})\sigma_3$ . It is renormalized by the diagram in Fig. 2a).

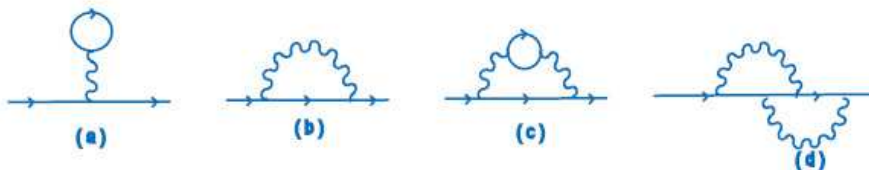


Figure 2. Feynman diagrams renormalizing the electron self-energy.

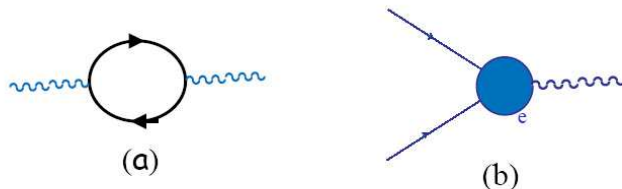


Figure 3. (a) Feynman diagram renormalizing the photon self-energy. (b) Vertex correction.

- The Fermi velocity renormalization. It is obtained already at the one loop level from the diagram in Fig. 2b).
- The quasiparticle lifetime  $\tau^{-1} \sim \lim_{\omega \rightarrow 0} \text{Im}\Sigma(\omega, \mathbf{k})$ . Its first contribution is at the two-loops level from diagrams 2c), 2d) in Fig. 2.
- The wave function renormalization  $Z_\Psi \sim \frac{\partial \Sigma(\omega, \mathbf{k})}{\partial \omega} \Big|_{\omega=0}$ , defines the anomalous dimension of the field  $\gamma = \partial \log Z_\Psi / \partial l$  ( $l$  is the RG parameter) and, hence of the fermion propagator:  $G(\omega, \mathbf{k}) \sim_{\omega \rightarrow 0} \frac{1}{\omega^\gamma}$ . It is a critical exponent that determines the universality class of the given model. Under the physical point of view it affects the interlayer tunneling and other transport properties.

The next set of diagrams to analyze corresponds to the photon self-energy and vertex corrections represented schematically in Fig. 3.

The real part of the photon self-energy at one loop (polarization) renormalizes the interaction and the imaginary part gives the density of electron-hole excitations of the system. The vertex corrections renormalize the electric charge.

### 3.3. Results.

In the computation of the diagrams mentioned it is readily seen that the loop corrections come in powers of an effective coupling constant given by  $g = e^2/4\pi v_F$ . The physical results extracted from the RG analysis are the following.

1. From the computation of the electron self-energy (Fig. 2b)) we get a non trivial renormalization of the Fermi velocity that **grows in the infrared**. This result implies a breakdown of the relation between the energy and momentum scaling, a signature of a quantum critical point.

2. From the electron self-energy at two loops order we get a non trivial wave function renormalization meaning that the infrared stable fixed point corresponds to a free fixed point different from the Fermi liquid. This result has been shown to persist in the non-perturbative regime[14]. This is a non-trivial result that has physical implications. In particular it implies that the inverse quasiparticle lifetime increases linearly with energy[4], a result that has been observed experimentally in [3] in the energy range of validity of the model.

3. The electron-photon vertex and the photon propagator are not renormalized at the one loop level. This means that the electric charge is not renormalized, a result that could be predicted by gauge invariance, and it also implies that the effective coupling constant  $g = e^2/4\pi v_F$  **decreases at low energies** defining an infrared free fixed point of the RG. It is interesting to note that the Lorentz invariance of the model that was explicitly broken by the Fermi velocity is recovered at the fixed point since the velocity of light,  $c$ , fixes a limit to the growing of the Fermi velocity. In conclusion, the RG analysis shows that without disorder, edges, or other perturbations, the graphene system at low energies has gapless excitations differing from the Fermi liquid quasiparticles but does not support magnetic or superconducting instabilities. It is interesting to note that the energy dependence of the coupling constant[14] can lead to non trivial scaling features in optical properties[16].

The strong coupling regime of the graphene system has been analyzed in [17]. There it is argued that a dynamical breakdown of the chiral symmetry (degeneracy between the two Fermi points) will occur at strong coupling and a gap will open in the spectrum forming a kind of charge density wave. Graphite can then be seen as an excitonic insulator that can become ferromagnetic upon doping. The resulting gap has an exponentially small non-perturbative value.

The analysis in this section neglects short range interactions, as their effects are less relevant than those arising from the long range Coulomb interaction. It is worth noting, however, that a sufficiently large on-site repulsion can induce a transition to an antiferromagnetic ground state[18], and that, even below this transition, significant effects at low energies can be expected[19].

## 4. Effects of disorder.

### 4.1. General features.

As mentioned elsewhere in this volume, there is a wide variety of carbon compounds, ranging from crystalline diamond, where the carbon atoms show fourfold coordination, to graphite, where the coordination is threefold, and the coupling between neighboring planes is weak. The environment around a carbon atom in nanotubes and the fullerenes is closer to the graphite case, although the bonds with the three nearest neighbors are distorted. The variety of possible environments around a carbon atom imply that many intermediate, metastable phases can exist. As in any other materials, disorder can appear due to lattice



defects or impurities. In the following, we consider the changes in the electronic states in threefold coordinated systems due to some simple lattice defects, like five- and sevenfold rings, vacancies, dislocations and edges. We will not address the stronger deformations associated with hybrid three- and fourfold bonding ( $sp^3 - sp^2$  hybridization) which may exist in highly disordered systems[2].

#### 4.2. Five- and sevenfold rings (disclinations).

As discussed earlier, the low energy electronic states of graphene planes are well described by a two dimensional Dirac equation, which reproduces correctly the semimetallic nature of the system. Some lattice distortions give rise to long range modifications in the electronic wavefunctions. These effects should be well described using the effective Dirac equation as a starting point.

The simplest defects which show these features are five- or sevenfold rings in the honeycomb lattice. These defects can be considered disclinations of the lattice, which acquires a finite curvature. The accumulation of them leads to curved shapes, like the fullerenes, which show twelve fivefold rings. Sevenfold rings lead to negative curvature, and a variety of compounds have been proposed to exist with this property[20]. A simple way to show that an odd numbered ring in the honeycomb lattice leads to long range effects in the electronic spectrum is by noting that any closed path which encompasses the defect leads to an interchange of the two sublattices which build the structure[7]. The description of the electronic states in terms of the Dirac equation is achieved by using two types of electronic “flavors”, each of them existing in a different sublattice. The existence of odd numbered rings changes the Dirac equation at any distance from the defect.

If we neglect for the moment the effect of the long range lattice distortions induced by these defects, the only consequence of the presence of odd numbered rings is the above mentioned interchange of the two sublattices. In the Dirac description it implies that, when moving around the defect, the two electronic flavors are exchanged. The standard way to associate to a translation a smooth change in other properties is through gauge potentials. The existence of a gauge potential implies, in general, that the usual derivative has to be replaced by the covariant derivative, which includes the potential. The usual derivative operator is the generator of a translation through the system. A covariant derivative with a finite gauge potential implies that, when translating an object, an additional operation has to be performed upon it. In the case considered here, this operation is a rotation in flavor space. As there are two flavors, the index which distinguishes them is equivalent to a spin one half. The rotations in this space build up the  $SU(2)$  non abelian group. The gauge potential needed has to be chosen such that the accumulated rotation in a path which encircles the defect should be independent of the path. Hence, the gauge potential is equivalent to that generated by a fixed “magnetic” flux at the position of the defect<sup>2</sup>.

A schematic view of the correspondence of a fivefold ring and a disclination is shown in Fig.[4]. The previous analysis shows that the effects on the electronic states of odd numbered rings in the honeycomb lattice are approximately described in terms of a gauge

---

<sup>2</sup>One must note that there is an additional technical complication, associated to the fact that there is also another index associated to the two inequivalent Fermi points in the Brillouin Zone. An odd numbered ring also exchanges them.

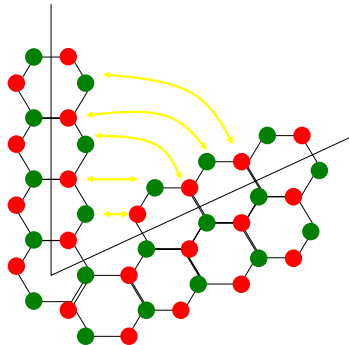


Figure 4. Description of a fivefold ring in the honeycomb structure in terms of a disclination. The identification of sites at the two edges imply a correspondence between sites from one sublattice and the other.

field which decays inversely proportional to the distance to the defect. This scheme allows us to calculate analytically the low energy electronic spectrum of closed structures, like  $C_{60}$  and higher fullerenes[7]. The comparison with more detailed calculations is quite reasonable, and, as expected, improves as the radius of the system becomes larger.

### 4.3. Dislocations.

The effects induced far away from the core of a dislocation can be approximated by assuming that the dislocation is made up of two disclinations of opposite sign. The general model of a disclination has been given in the previous section, and it can be directly applied to the case of a dislocation. Its effect on the low energy electronic spectrum can be approximated by the gauge field induced by two opposite magnetic fluxes separated by a distance of the order of the Burgers vector of the dislocation. This field decays like the inverse of the square of the distance to the defect.

### 4.4. Edge states.

Tight binding models have shown that, in the vicinity of the edges of graphene planes, localized states at zero energy can exist[21,22]. These states are well described by the Dirac equation used here. The existence of a state at zero energy implies the existence of a localized wavefunction  $(\Psi_1(\tilde{\mathbf{r}}), \Psi_2(\tilde{\mathbf{r}}))$  such that:

$$\begin{aligned} (\partial_x + i\partial_y) \Psi_1(\tilde{\mathbf{r}}) &= 0 \\ (\partial_x - i\partial_y) \Psi_2(\tilde{\mathbf{r}}) &= 0 \end{aligned} \tag{11}$$

These equations are satisfied if  $\Psi_1(\tilde{\mathbf{r}})$  is an analytic function of  $z = x + iy$  and  $\Psi_2(\tilde{\mathbf{r}}) = 0$ , or if  $\Psi_1(\tilde{\mathbf{r}}) = 0$  and  $\Psi_2(\tilde{\mathbf{r}})$  is an analytic function of  $\bar{z} = x - iy$ . We now consider a semiinfinite

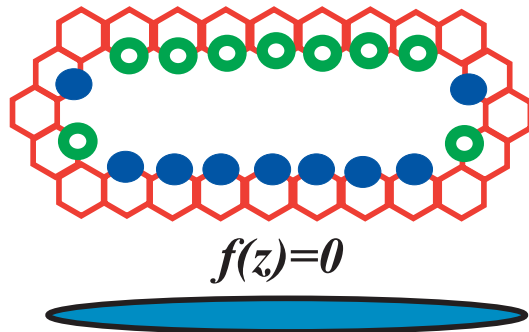


Figure 5. Elongated crack in the honeycomb structure. The crack is such that the sites in the upper edge belong to one sublattice, while those at the lower edge belong to the other. Bottom: approximate cut in the complex plane which can be used to represent this crack at long distances.

honeycomb lattice with an edge at  $y = 0$  and which occupies the half plane  $x > 0$ . A possible solution which decays as  $x \rightarrow \infty$  is  $\Psi_1(x, y) \propto e^{-kz} = e^{iky} e^{-kx}$ ,  $\Psi_2(\tilde{\mathbf{r}}) = 0$ . These solutions satisfy the boundary conditions at  $y = 0$  if the last column of carbon atoms belong to the sublattice where the component  $\Psi_1$  is defined. Then, the next column belongs to the other sublattice, where the amplitude of the state is, by construction, zero.

#### 4.5. Vacancies.

The analysis in the previous section of edge states can be extended to the existence of localized states near extended vacancies in the honeycomb lattice. The only possible localized states can exist at zero energy, where the density of extended states vanishes. Then, the wavefunctions obtained from the Dirac equations must be normalizable and analytic on the variables  $z = x + iy$  or  $\bar{z} = x - iy$ . Extended vacancies with approximate circular shape can support solutions of the type  $\Psi(\tilde{\mathbf{r}}) \propto z^{-n}$ ,  $n > 1$ . By using conformal mapping techniques, solutions can be found with the boundary conditions appropriate to the shape of different defect.

A simple case is the elongated crack depicted in Fig.[5]. A localized solution is described by an analytic function  $f(z)$  such that  $\text{Re}f(z) = 0$  at the edges of the crack. A family of functions for a crack of half length  $L$ , which satisfy these requirements are:

$$f(z) = \frac{1}{(z^2 - L^2)^{n+1/2}} \quad (12)$$

#### 4.6. Random distribution of defects.

As discussed above, many classes of lattice defects can be described by gauge fields coupled to the two dimensional Dirac equation. A random distribution of defects leads to a random gauge field, with variance related to the type of defect and its concentration. There is an extensive literature on the problem, as the model is also relevant to Fractional Quantum Hall states and to disorder in d-wave superconductors. A random field, when

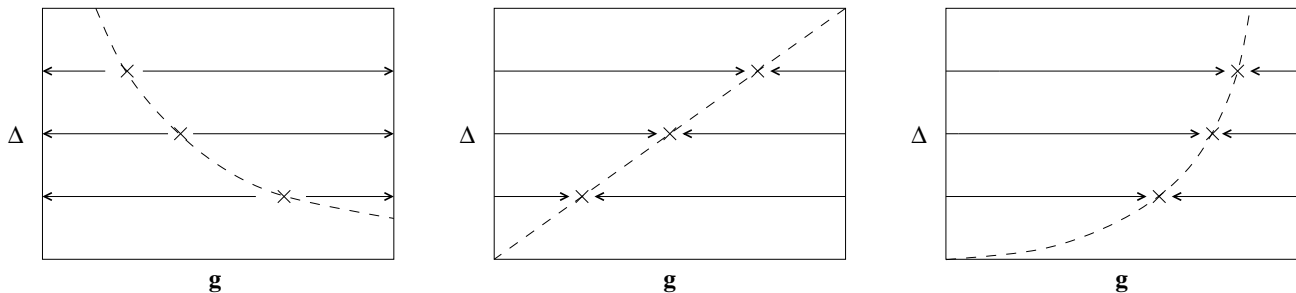


Figure 6. Phase diagram calculated by renormalizing the strength of the disorder,  $\Delta$ , and the Coulomb interaction,  $g$ , at the same time. The three plots correspond to three types of disorder. Left: random on site potential. Center: Random disorder in the lattice structure. Right: Random correction to the hoppings.

treated perturbatively, leads to corrections to the wavefunction renormalization which depend logarithmically in the electronic bandwidth, in the same manner as the corrections induced by the long range Coulomb interaction. Hence, disorder is a marginal perturbation in the Renormalization Group sense, and can be analyzed using the same approach employed in the study of the Coulomb interactions.

Disorder in systems with energy gaps tends to induce localized states inside the gap. The honeycomb lattice has a semimetallic density of states. A random field enhances the density of states at low energies, although the system preserves its semimetallic character. The density of states at low energies is changed from  $D(\omega) \propto |\omega|$  to  $D(\omega) \propto |\omega|^{1-\delta}$ , where  $\delta$  depends on the type of disorder[23,24,25].

## 5. Combined effects of disorder and the electronic interactions.

### 5.1. The long range Coulomb interaction.

The analysis of the Renormalization Group results presented previously led to the conclusion that the pure graphene system at low energies is an anomalous Fermi liquid with no short range interactions. Inclusion of disorder modelled as random gauge fields modifies the flow of the couplings and gives rise to new phases with different physical properties. Similar problems have been considered in relation to transitions between Fractional Quantum Hall states[26]. There the different types of "extended" disorder are associated to different gauge couplings that can be treated with the Renormalization Group technique together with the long range Coulomb interaction.

The values of the effective coupling constants at low energies are modified by the new interactions giving rise to a rich phase diagram with new phases with different physics depending of the type of disorder A schematic plot of the flow obtained for different types of disorder is shown in Fig.[6]. The most interesting phase is the one induced by the presence of random disorder in the lattice structure(center). It shows the existence of new phases, where the effect of the Coulomb interaction, which tends to lower the density of states at the Fermi energy [27], and the disorder, which has the opposite tendency, balance

each other. This phase is stable, within the limitations of the calculation presented here, for certain types of disorder[6].

## 5.2. Short range interactions.

As mentioned earlier, short range interactions, such as an onsite Hubbard term  $U$  are irrelevant, in the sense that their effect can be analyzed within standard perturbation theory without encountering divergences. This is due to the vanishing density of states at the Fermi level. The Hubbard model at half filling, in a two dimensional square lattice leads to a highly singular perturbation expansion, due to the diverging density of states at the Fermi level. As mentioned above, the density of states at low energies is increased by the presence of disorder. This, in turn, enhances the effect of short range interactions.

Short range interactions can lead to a variety of phases at low temperatures. In the absence of disorder, an onsite Hubbard term favors antiferromagnetism. An antiferromagnetic phase, however, is likely to be suppressed by disorder, especially by the presence of odd numbered rings in the lattice. Then, the next leading instability that such an interaction can induce is towards a ferromagnetic phase.

If a magnetic phase does not appear, electron-electron interactions, even when they are repulsive, will lead to an anisotropic ground state. The existence of two inequivalent Fermi points in the Brillouin zone suggests that the superconducting order parameter induced by a repulsive interaction will have opposite sign at each point. The corresponding symmetry is p-wave. No that disorder, in addition to the enhancement of the density of states mentioned already, will lead to pair breaking effects in an anisotropic superconducting phase.

## 5.3. Interactions between localized states.

As mentioned in the previous section, vacancies and cracks in the honeycomb lattice induce localized states at the Fermi energy. These states will become polarized in the presence of repulsive interactions, as this polarization implies no cost of kinetic energy. Then, we can expect that lattice defects will nucleate magnetic moments in their vicinity. These moments can be large, as the number of localized states is proportional to the number of sites at the perimeter of the defect. Note that this mechanism is intrinsic to the graphene structure, and it does not require the trapping of magnetic ions near the defects.

The moments near different defects polarize the conduction band of the surrounding medium, leading to an effective RKKY interaction. In an ordinary metal this interaction is made up of an oscillatory and a decaying term as function of distance, and it can be of either sign, leading to frustration and spin glass effects. The graphene plane considered here, however, does not have a Fermi surface, so that the induced RKKY interaction does not oscillate. A simple analysis, using the analytical expression for the susceptibility discussed in earlier chapters, gives:

$$J_{RKKY}(\tilde{\mathbf{r}}) \sim U^2 \int d^2\mathbf{k} e^{i\tilde{\mathbf{k}}\tilde{\mathbf{r}}} \chi(\tilde{\mathbf{k}}) \sim U^2 \frac{a^4}{v_F |\tilde{\mathbf{r}}|^3} \quad (13)$$

where  $U$  is the magnitude of the onsite Hubbard term. Hence, the RKKY interaction is ferromagnetic, and it decays as  $r^{-3}$  as function of the distance between local moments.

## 6. Coupling between graphene layers.

### 6.1. Coulomb interactions.

So far, we have considered the properties of isolated graphene layers. As the source of most of the unusual properties reported here is the long ranged Coulomb interaction, it is important to consider the screening effects of neighboring layers.

The calculation of the full dielectric constant of a set of metallic or semimetallic layers in terms of single layer properties can be done analytically. The dielectric function of the system can be written as[5]:

$$\frac{1}{\epsilon(\tilde{\mathbf{q}}, \omega)} = \frac{\sinh(|\tilde{\mathbf{q}}|d)}{\sqrt{[\cosh(|\tilde{\mathbf{q}}|d) + (2\pi e^2/|\tilde{\mathbf{q}}|) \sinh(|\tilde{\mathbf{q}}|d) \chi_0(\tilde{\mathbf{q}}, \omega)]^2 - 1}} \quad (14)$$

where  $\chi_0(\tilde{\mathbf{q}}, \omega)$  is the charge response function of an isolated layer, and  $d$  is the interlayer distance. This response function is finite for  $|\tilde{\mathbf{q}}| \ll d^{-1}$ , so that the interactions remain long range.

### 6.2. Interlayer hopping.

The electron–electron interaction modifies the quasiparticle propagator, as discussed above. The electrons within the layers are dressed by a cloud of virtual excitations. This cloud cannot follow an electron which hops between neighboring layers, reducing the effective tunnelling element.

In conventional Fermi liquids, this renormalization of the interlayer hopping is finite, and it can be calculated using perturbation theory. In the model studied here, this calculation leads to divergencies, and it resembles closely the analysis of the electron self energy sketched previously.

The “orthogonality catastrophe ” which results from the virtual excitation of electron-hole pairs has been extensively discussed in connection to the physics of mesoscopic systems[28], and it has also been applied to the related problem of tunnelling between two dirty metallic layers[29]. Similar procedures can be used in the present case. The interlayer hopping acquires a multiplicative renormalization which makes it vanish at low energies, even in clean samples. This calculation is consistent with the extreme anisotropy observed in some experiments[8].

## 7. Conclusions.

We have discussed a simplified model for the long wavelength electronic properties of graphene planes. The interplay between the semimetallic properties of the planes and the long range interactions leads to the existence of a variety of interesting effects:

- The model, in the absence of disorder, shows deviations from Landau’s theory of a Fermi liquid. The quasiparticles are strongly renormalized, and their lifetimes do not follow the usual  $\Gamma(\epsilon) \propto (\epsilon - \epsilon_F)^2$  behavior. The low energy electronic properties of the system can be thought as similar to the “pseudogap ” regime in the superconducting cuprates.
- Disorder can be incorporated into the model in a simple way. While the interactions tend to deplete the electronic density of states near the Fermi energy, disorder

leads to its enhancement. The resulting competition induces the existence of an “incoherent metal ” regime at low energies, similar to the one dimensional Luttinger liquid, although stabilized by the disorder.

- Large lattice deformations can nucleate localized electronic states in their vicinity<sup>3</sup>. These states can lead to the formation of local moments. The absence of a finite Fermi wavevector implies that the RKKY interaction mediated by the conduction electrons does not change sign, and it is ferromagnetic. Hence, the frustration which leads to spin glass behavior in metals with magnetic impurities is absent in this case.
- The screening cloud around quasiparticles suppresses interlayer tunnelling, enhancing the anisotropy of the electronic properties.

## REFERENCES

1. J. C. Slonczewski and P. R. Weiss, Phys. Rev. **109**, 272 (1958).
2. A. A. Ovchinnikov and I. L. Shamovsky, Journ. of. Mol. Struc. (Theochem) **251**, 133 (1991).
3. S. Yu, J. Cao, C. C. Miller, D. A. Mantell, R. J. D. Miller, and Y. Gao, Phys. Rev. Lett. **76**, 483 (1996).
4. J. González, F. Guinea and M. A. H. Vozmediano, Phys. Rev. Lett. **77**, 3589 (1996).
5. J. González, F. Guinea, and M. A. H. Vozmediano Phys. Rev. B **63**, 134421 (2001)
6. T. Stauber, F. Guinea, and M. A. H. Vozmediano, *Phys. Rev. B.* **71** R041406 (2005).
7. J. González, F. Guinea and M. A. H. Vozmediano, Phys. Rev. Lett. **69**, 172 (1992), Nucl. Phys. **B406**, 771 (1993).
8. R. Ocaña, P. Esquinazi, H. Kempa, J. H. S. Torres, and Y. Kopelevich, Phys. Rev. B **68**, 165408 (2003).
9. M. A. H. Vozmediano, M. P. López-Sancho, and F. Guinea Phys. Rev. Lett. **89**, 166401 (2002). *ibid* Phys. Rev. B **68**, 195122 (2003).
10. R. Saito, G. Dresselhaus, and M.S. Dresselhaus, 'Physical Properties of Carbon Nanotubes' (Imperial College Press, London, 1998).
11. R. Shankar, Rev. Mod. Phys. **66** (1994) 129.
12. J. Polchinski, in **Proceedings of the 1992 TASI in Elementary Particle Physics**, J. Harvey and J. Polchinski eds. (World Scientific, Singapore, 1992).
13. J. Solyom, Adv. Phys. **28**, 201 (1079).
14. J. González, F. Guinea and M. A. H. Vozmediano, Phys. Rev. B, **59** R2474 (1999).
15. J. González, F. Guinea and M. A. H. Vozmediano, Mod. Phys. Lett. **B7**, 1593 (1994), *ibid*, Nucl. Phys. B **424**, 595 (1994), *ibid*, Journ. Low. Temp. Phys. **99**, 287 (1995).
16. C. L. Kane and E. J. Mele, Phys. Rev. Lett. **93**, 197402 (2004).
17. D. V. Khveshchenko, Phys. Rev. Lett. **87**, 48246802 (2001); *ibid*, Phys. Rev. Lett. **87**, 48246802 (2001).
18. S. Sorella and E. Tosatti, Europhys. Lett. **19** 699 (1992).

---

<sup>3</sup>Note that these states are built up from the  $\pi$  orbitals of each layer, and the  $\sigma$  bonds remain unaltered.

19. G. Baskaran and S. A. Jafari, Phys. Rev. Lett. **89**, 016402 (2002); N. M. R. Peres, M. A. N. Araújo, and A. H. Castro Neto, Phys. Rev. Lett. **92**, 199701 (2004); G. Baskaran and S. A. Jafari, Phys. Rev. Lett. **92**, 199702 (2004); N. M. R. Peres, A. H. Castro Neto, and F. Guinea, to be published.
20. D. Vanderbilt and J. Tersoff, Phys. Rev. Lett. **68**, 511 (1992). J. L. Aragón, H. Terrones, and D. Romeu, Phys. Rev. B **48**, 8409 (1993).
21. K. Wakayabashi and M. Sigrist, Phys. Rev. Lett. **84**, 3390 (2000).
22. K. Wakayabashi, Phys. Rev. B **64**, 125428 (2001).
23. C. de C. Chamon, C. Mudry and X.-G. Wen, Phys. Rev. B **53**, R7638 (1996).
24. H. E. Castillo, C. de C. Chamon, E. Fradkin, P. M. Goldbart and C. Mudry, Phys. Rev. B **56**, 10668 (1997).
25. B. Horovitz and P. Le Doussal, Phys. Rev. B **65**, 125323 (2002).
26. J. Ye, Phys. Rev. B **60**, 8290 (1999).
27. M.P. López-Sancho, M.C. Muñoz, and L. Chico, Phys. Rev. B **63**, 165419 (2001).
28. E. Bascones, C. P. Herrero, F. Guinea, and G. Schön, Phys. Rev. B **61**, 16778 (2000).
29. M. Turlakov and A. J. Leggett, Phys. Rev. B **63**, 064518 (2001).